Nonlinear optical properties of multilayer graphene in the infrared

Giorgos Demetriou,[1] Henry T. Bookey,[1,2] Fabio Biancalana,[1] Eitan Abraham,[1] Yu Wang,[3] Wei Ji,[4] and Ajoy K. Kar[1,*]

[1]*Institute of Photonics and Quantum Sciences, School of Engineering and Physical Sciences, David Brewster Building, Heriot-Watt University, Edinburgh, EH14 4AS, UK*

[2]*Fraunhofer Centre for Applied Photonics, 99 George Street, Technology and Innovation Centre, Glasgow G1 1RD, UK*

[3]*State Key Laboratory of Multiphase Complex Systems, Institute of Process Engineering, Chinese Academy of Sciences, Beijing 100190, China*

[4]*Department of Physics, National University of Singapore, 2 Science Drive 3, Singapore 117542, Singapore*

[*]*a.k.kar@hw.ac.uk*

Abstract: A negative value for the nonlinear refraction in graphene is experimentally observed and unambiguously verified by performing a theoretical analysis arising from the conductivity of the graphene monolayer. The nonlinear optical properties of multi-layer graphene are experimentally studied by employing the Z-scan technique. The measurements are carried out at 1150, 1550, 1900 and 2400 nm with a 100-femtosecond laser source. Under laser illumination the multi-layer graphene exhibits a transmittance increase due to saturable absorption, followed by optical limiting due to two-photon absorption. The saturation irradiance I_{sat} and the two-photon absorption coefficient β are measured in the operating wavelength range. Furthermore, an irradiance-dependent nonlinear refraction is observed and discriminated from the conventional nonlinear refraction coefficient $n_{2,}$ which is not irradiance dependent. The values obtained for the irradiance-dependent nonlinear refraction are in the order of ~10^{-9} cm^2W^{-1}, approximately 8 orders of magnitude larger than any bulk dielectrics.

OCIS codes: (160.4330) Nonlinear optical materials; (320.7110) Ultrafast nonlinear optics.

References and links

1. F. Bonaccorso, Z. Sun, T. Hasan, and A. C. Ferrari, "Graphene photonics and optoelectronics," Nat. Photonics **4**(9), 611–622 (2010).
2. K. S. Novoselov, A. K. Geim, S. V. Morozov, D. Jiang, Y. Zhang, S. V. Dubonos, I. V. Grigorieva, and A. A. Firsov, "Electric Field Effect in Atomically Thin Carbon Films," Science **306**(5696), 666–669 (2004).
3. F. H. L. Koppens, T. Mueller, P. Avouris, A. C. Ferrari, M. S. Vitiello, and M. Polini, "Photodetectors based on graphene, other two-dimensional materials and hybrid systems," Nat. Nanotechnol. **9**(10), 780–793 (2014).
4. T. Hasan, Z. Sun, F. Wang, F. Bonaccorso, P. H. Tan, A. G. Rozhin, and A. C. Ferrari, "Nanotube–Polymer Composites for Ultrafast Photonics," Adv. Mater. **21**(38), 3874–3899 (2009).
5. Z. Sun, T. Hasan, F. Torrisi, D. Popa, G. Privitera, F. Wang, F. Bonaccorso, D. M. Basko, and A. C. Ferrari, "Graphene Mode-Locked Ultrafast Laser," ACS Nano **4**(2), 803–810 (2010).
6. J. Wang, Y. Hernandez, M. Lotya, J. N. Coleman, and W. J. Blau, "Broadband Nonlinear Optical Response of Graphene Dispersions," Adv. Mater. **21**(23), 2430–2435 (2009).
7. S. A. Mikhailov, "Theory of the nonlinear optical frequency mixing effect in graphene," Physica E **44**(6), 924–927 (2012).
8. M. Dragoman, D. Neculoiu, G. Deligeorgis, G. Konstantinidis, D. Dragoman, A. Cismaru, A. A. Muller, and R. Plana, "Millimeter-wave generation via frequency multiplication in graphene," Appl. Phys. Lett. **97**(9), 093101 (2010).
9. H. Wang, A. Hsu, K. Kang, J. Kong, and T. Palacios, "Gigahertz ambipolar frequency multiplier based on CVD graphene," in *Electron Devices Meeting (IEDM), 2010 IEEE International*, 2010), 23.26.21–23.26.24.

#261726 Received 23 Mar 2016; revised 29 May 2016; accepted 30 May 2016; published 6 Jun 2016

Corrected: 07 June 2016

10. R. Mary, G. Brown, S. J. Beecher, F. Torrisi, S. Milana, D. Popa, T. Hasan, Z. Sun, E. Lidorikis, S. Ohara, A. C. Ferrari, and A. K. Kar, "1.5 GHz picosecond pulse generation from a monolithic waveguide laser with a graphene-film saturable output coupler," Opt. Express **21**(7), 7943–7950 (2013).
11. D. Popa, Z. Sun, T. Hasan, F. Torrisi, F. Wang, and A. C. Ferrari, "Graphene Q-switched, tunable fiber laser," Appl. Phys. Lett. **98**(7), 073106 (2011).
12. Z. Sun, D. Popa, T. Hasan, F. Torrisi, F. Wang, E. R. Kelleher, J. Travers, V. Nicolosi, and A. Ferrari, "A stable, wideband tunable, near transform-limited, graphene-mode-locked, ultrafast laser," Nano Res. **3**(9), 653–660 (2010).
13. R. Yingying, G. Brown, R. Mary, G. Demetriou, D. Popa, F. Torrisi, A. C. Ferrari, C. Feng, and A. K. Kar, "7.8-GHz Graphene-Based 2-μm Monolithic Waveguide Laser," IEEE J. Sel. Top. Quantum Electron. **21**(1), 395–400 (2015).
14. D. Popa, Z. Sun, F. Torrisi, T. Hasan, F. Wang, and A. C. Ferrari, "Sub 200 fs pulse generation from a graphene mode-locked fiber laser," Appl. Phys. Lett. **97**(20), 203106 (2010).
15. Q. Bao, H. Zhang, Y. Wang, Z. Ni, Y. Yan, Z. X. Shen, K. P. Loh, and D. Y. Tang, "Atomic-Layer Graphene as a Saturable Absorber for Ultrafast Pulsed Lasers," Adv. Funct. Mater. **19**(19), 3077–3083 (2009).
16. H. Zhang, Q. Bao, D. Tang, L. Zhao, and K. Loh, "Large energy soliton erbium-doped fiber laser with a graphene-polymer composite mode locker," Appl. Phys. Lett. **95**(14), 141103 (2009).
17. H. Zhang, D. Y. Tang, L. M. Zhao, Q. L. Bao, and K. P. Loh, "Large energy mode locking of an erbium-doped fiber laser with atomic layer graphene," Opt. Express **17**(20), 17630–17635 (2009).
18. W. B. Cho, J. W. Kim, H. W. Lee, S. Bae, B. H. Hong, S. Y. Choi, I. H. Baek, K. Kim, D.-I. Yeom, and F. Rotermund, "High-quality, large-area monolayer graphene for efficient bulk laser mode-locking near 1.25 μm," Opt. Lett. **36**(20), 4089–4091 (2011).
19. M. N. Cizmeciyan, J. W. Kim, S. Bae, B. H. Hong, F. Rotermund, and A. Sennaroglu, "Graphene mode-locked femtosecond Cr:ZnSe laser at 2500 nm," Opt. Lett. **38**(3), 341–343 (2013).
20. F. Xing, G.-X. Meng, Q. Zhang, L.-T. Pan, P. Wang, Z.-B. Liu, W.-S. Jiang, Y. Chen, and J.-G. Tian, "Ultrasensitive Flow Sensing of a Single Cell Using Graphene-Based Optical Sensors," Nano Lett. **14**(6), 3563–3569 (2014).
21. H. Yang, X. Feng, Q. Wang, H. Huang, W. Chen, A. T. S. Wee, and W. Ji, "Giant Two-Photon Absorption in Bilayer Graphene," Nano Lett. **11**(7), 2622–2627 (2011).
22. D. Sun, C. Divin, J. Rioux, J. E. Sipe, C. Berger, W. A. de Heer, P. N. First, and T. B. Norris, "Coherent Control of Ballistic Photocurrents in Multilayer Epitaxial Graphene Using Quantum Interference," Nano Lett. **10**(4), 1293–1296 (2010).
23. W. Chen, Y. Wang, and W. Ji, "Two-Photon Absorption in Graphene Enhanced by the Excitonic Fano Resonance," J. Phys. Chem. C **119**(29), 16954–16961 (2015).
24. M. Sheik-Bahae, A. A. Said, T. H. Wei, D. J. Hagan, and E. W. Van Stryland, "Sensitive measurement of optical nonlinearities using a single beam," IEEE J. Quantum Electron. **26**(4), 760–769 (1990).
25. H. Zhang, S. Virally, Q. Bao, L. K. Ping, S. Massar, N. Godbout, and P. Kockaert, "Z-scan measurement of the nonlinear refractive index of graphene," Opt. Lett. **37**(11), 1856–1858 (2012).
26. E. Hendry, P. J. Hale, J. Moger, A. K. Savchenko, and S. A. Mikhailov, "Coherent Nonlinear Optical Response of Graphene," Phys. Rev. Lett. **105**(9), 097401 (2010).
27. C. Q. Xia, C. Zheng, M. S. Fuhrer, and S. Palomba, "Nonlinear optical frequency mixing response of single and multilayer graphene," Opt. Lett. **41**(6), 1122–1125 (2016).
28. K. J. A. Ooi, L. K. Ang, and D. T. H. Tan, "Waveguide engineering of graphene's nonlinearity," Appl. Phys. Lett. **105**(11), 111110 (2014).
29. S. Ghosh, W. Bao, D. L. Nika, S. Subrina, E. P. Pokatilov, C. N. Lau, and A. A. Balandin, "Dimensional crossover of thermal transport in few-layer graphene," Nat. Mater. **9**(7), 555–558 (2010).
30. E. Pop, V. Varshney, and A. K. Roy, "Thermal properties of graphene: Fundamentals and applications," MRS Bull. **37**(12), 1273–1281 (2012).
31. A. A. Balandin, S. Ghosh, W. Bao, I. Calizo, D. Teweldebrhan, F. Miao, and C. N. Lau, "Superior Thermal Conductivity of Single-Layer Graphene," Nano Lett. **8**(3), 902–907 (2008).
32. H. Harutyunyan, R. Beams, and L. Novotny, "Controllable optical negative refraction and phase conjugation in graphite thin films," Nat. Phys. **9**(7), 423–425 (2013).
33. J. B. Pendry, "Negative Refraction Makes a Perfect Lens," Phys. Rev. Lett. **85**(18), 3966–3969 (2000).
34. N. Fang, H. Lee, C. Sun, and X. Zhang, "Sub-Diffraction-Limited Optical Imaging with a Silver Superlens," Science **308**(5721), 534–537 (2005).
35. T. Taubner, D. Korobkin, Y. Urzhumov, G. Shvets, and R. Hillenbrand, "Near-Field Microscopy Through a SiC Superlens," Science **313**(5793), 1595 (2006).
36. X. Li, W. Cai, J. An, S. Kim, J. Nah, D. Yang, R. Piner, A. Velamakanni, I. Jung, E. Tutuc, S. K. Banerjee, L. Colombo, and R. S. Ruoff, "Large-Area Synthesis of High-Quality and Uniform Graphene Films on Copper Foils," Science **324**(5932), 1312–1314 (2009).
37. S. Bae, H. Kim, Y. Lee, X. Xu, J.-S. Park, Y. Zheng, J. Balakrishnan, T. Lei, H. R. Kim, Y. I. Song, Y.-J. Kim, K. S. Kim, B. Ozyilmaz, J.-H. Ahn, B. H. Hong, and S. Iijima, "Roll-to-roll production of 30-inch graphene films for transparent electrodes," Nat. Nanotechnol. **5**(8), 574–578 (2010).
38. J. Wang, B. Gu, H.-T. Wang, and X.-W. Ni, "Z-scan analytical theory for material with saturable absorption and two-photon absorption," Opt. Commun. **283**(18), 3525–3528 (2010).

#261726 Received 23 Mar 2016; revised 29 May 2016; accepted 30 May 2016; published 6 Jun 2016

39. Y. Gao, X. Zhang, Y. Li, H. Liu, Y. Wang, Q. Chang, W. Jiao, and Y. Song, "Saturable absorption and reverse saturable absorption in platinum nanoparticles," Opt. Commun. **251**(4-6), 429–433 (2005).
40. B. S. Kalanoor, P. B. Bisht, S. Akbar Ali, T. T. Baby, and S. Ramaprabhu, "Optical nonlinearity of silver-decorated graphene," J. Opt. Soc. Am. B **29**(4), 669–675 (2012).
41. S. Husaini, J. E. Slagle, J. M. Murray, S. Guha, L. P. Gonzalez, and R. G. Bedford, "Broadband saturable absorption and optical limiting in graphene-polymer composites," Appl. Phys. Lett. **102**(19), 191112 (2013).
42. L. A. Falkovsky, "Optical properties of graphene," J. Phys. Conf. Ser. **129**, 012004 (2008).
43. T. Gu, N. Petrone, J. F. McMillan, A. van der Zande, M. Yu, G. Q. Lo, D. L. Kwong, J. Hone, and C. W. Wong, "Regenerative oscillation and four-wave mixing in graphene optoelectronics," Nat. Photonics **6**(8), 554–559 (2012).
44. E. Malic and A. Knorr, *Graphene and Carbon Nanotubes: Ultrafast Optics and Relaxation Dynamics* (Wiley, Berlin, 2013).

1. Introduction

Graphene has a number of remarkable optoelectronic properties resulting from its unique band structure [1,2]. The linear dispersion of the massless Dirac fermions implies that graphene can absorb photons with the same efficiency over a wide range of wavelengths. These properties, combined with the high carrier mobility as well as mechanical and thermal properties make graphene an ideal candidate for a wide range of optoelectronic applications [1–3].

The nonlinear optical properties of graphene associated with saturable absorption (SA) [4,5], optical limiting [6], frequency mixing [7] and frequency multiplication [8,9] are attracting increasing interest due to the possible applications in ultrafast lasers [5,10–19] and optical sensors [20]. Saturable absorption is a consequence of Pauli blocking, when carriers generated because of strong optical excitation lead to the depletion of the valence band and the filling of the conduction band, preventing additional absorption. This property has led to the utilization of graphene as a saturable absorber for mode-locked and Q-switched lasers [5,10–19]. Recently, two-photon absorption (2PA) in graphene has also received attention [21–23]. Thus, there is interest in investigating the nonlinear optical properties of graphene and more specifically the relationship between SA and 2PA in order to optimize the design of devices based upon them.

Here we fabricated a high-quality, large-area multi-layer (5-7 layers) graphene sample to investigate its nonlinear optical response in the femtosecond regime at 1150, 1550, 1900 and 2400 nm by employing the Z-scan technique [24]. Z-scan, a technique which is based on the principles of spatial distortion of a focused Gaussian beam by a sample translated along its propagation path, offers both great simplicity and very high sensitivity upon measuring the optical nonlinearities of the sample in question. Under strong laser illumination the multilayer graphene exhibits a transmittance increase due to saturable absorption, followed by a decrease in transmittance leading to an optical limiting effect due to 2PA. Particularly in the case of graphene which presents both saturable and two-photon absorption, Z-scan is a fast and elegant way to discriminate the SA and 2PA processes and investigate the threshold at which SA turns to 2PA. Furthermore, it enables to unambiguously determine the 2PA coefficients, β, and the saturation irradiances, I_{sat}, in the operating wavelength range.

Furthermore, a nonlinear refraction effect is observed. This effect is irradiance-dependent due to the absorption saturation mechanism in graphene. Therefore we define this effect as irradiance-dependent nonlinear refraction and use the symbol, $\tilde{n}(I)$ discriminating it from the conventional n_2, which would indicate an irradiance-independent nonlinear refraction coefficient. More specifically, as the irradiance is increased the nonlinear refraction saturates. In this high irradiance regime, aside from $\chi_{gr}^{(3)}$ higher order odd terms of the nonlinear susceptibility, such as $\chi_{gr}^{(5)}$, $\chi_{gr}^{(7)}$ and so on become significant leading to the irradiance dependence of the nonlinear refraction. Thus making the conventional n_2 coefficient

#261726 Received 23 Mar 2016; revised 29 May 2016; accepted 30 May 2016; published 6 Jun 2016

unsuitable to describe the nonlinear refraction since it is only related to the $\chi_{gr}^{(3)}$ term of the nonlinear susceptibility.

The nonlinear optical Kerr effect of few-layer graphene has previously been reported by Zhang *et al.* [25]. In that work they performed Z-scan measurements by using 3.8 ps pulses at 1550 nm operating at a high repetition rate of 10 MHz. They reported a giant nonlinear refractive index, almost 9 orders of magnitude larger than bulk dielectrics, also pointing out its irradiance-dependence. It is precisely this exceptionally large value that leads to the contribution of higher order odd terms of the nonlinear susceptibility and subsequently the irradiance dependence of the nonlinear optical refraction in graphene as discussed in the previous paragraph. Furthermore, broadband four-wave mixing in few-layer graphene has been reported [26,27]. This allowed the determination of the absolute value of the third order susceptibility for a single graphene layer, $\left|\chi_{gr}^{(3)}\right| \cong 1.5\times10^{-7}$ esu, approximately 8 orders of magnitude larger than bulk dielectrics, further pointing out the giant nonlinear refraction in graphene. The value of $\left|\chi_{gr}^{(3)}\right| \cong 1.5\times10^{-7}$ esu reported in [26] corresponds to an equivalent n_2 of 1.5×10^{-9} $\mathrm{cm^2W^{-1}}$ [25]. However, the high repetition rate and long pulse duration employed in [25] could lead to an uncertainty in excluding nonlinear mechanisms of thermal nature.

In this work we investigate the nonlinear optical Kerr effect of few-layer graphene in the femtosecond temporal regime to a broad range of wavelengths, namely from 1150 nm to 2400 nm. Most importantly we show that the nonlinear refraction of graphene is negative. We operate in a low repetition rate regime of 1 kHz with 100 fs pulse durations to avoid any contribution from thermal effects. The negative value of the nonlinear refraction is supported with a theoretical analysis arising from the conductivity of the graphene monolayer, proving that graphene presents a negative nonlinear refraction over a broad range of wavelengths, as also pointed out by Ooi *et al.* [28]. Moreover, a thermal analysis confirms that there are no thermal contributions to the optical nonlinearity. The thermal analysis considers the temperature dynamics of a single layer. Since each layer absorbs the same fraction of the incident irradiance (2.3%), the temperature profiles for all layers will be identical. Furthermore, over the 100 fs pulse width used here, lateral diffusion can be neglected and therefore heat diffusion will occur at the same time in all layers. Moreover, there is no transverse temperature gradient, so diffusion occurs independently within each layer. The diffusion coefficient of graphene is given by $D_g \equiv k_g / \left(c_g \rho_g\right)$ where k_g is the in-plane thermal conductivity of graphene, c_g is the specific heat and ρ_g is the density of graphene. By using a modest value for the in-plane thermal conductivity of graphene in the order of $k_g \cong 10^3$ $\mathrm{WK^{-1}m^{-1}}$ [29] and taking the density of graphene as $\rho_g = 2.25\,\mathrm{gcm^{-3}}$ [30] and the specific heat as $c_g = 0.7\,\mathrm{JK^{-1}g^{-1}}$ [30], we obtained a diffusion coefficient, $D_g \cong 6.35$ $\mathrm{cm^2s^{-1}}$. Therefore, the 1 kHz repetition rate used in this work yields a diffusion length of 827 μm between successive pulses. The beam waists were measured at each of the operating wavelengths using the knife-edge technique and were found to be between 25 and 31 μm. This means that the diffusion length is ~31 times bigger than the beam waists, leading to a drop of the peak temperature by about three orders of magnitude before the next pulse arrives on the sample, therefore not enabling the manifestation of any thermal accumulation effects. Note that if a higher value for the thermal conductivity is used, in the orders of the superior thermal conductivity reported for single-layer graphene [31], it will yield a longer diffusion length and consequentially will lead to an even bigger drop of the peak temperature between successive pulses.

A negative refraction in graphite thin films using degenerate four-wave mixing has also been reported by Harutyunyan *et al.* [32]. Although due to the complexity of the technique

#261726 Received 23 Mar 2016; revised 29 May 2016; accepted 30 May 2016; published 6 Jun 2016

used in that work, it could not be unambiguously verified whether the negative refraction arose from the graphite films or the two counter-propagating beams forming a phase conjugating surface on the graphite films. This negative refraction property, which was experimentally studied in a broad wavelength range and explained theoretically in this work, defines graphene as a promising medium for super-resolution imaging [33–35].

2. Sample preparation

The sample is prepared as follows. Large-area (0.8×1.0 cm^2), multilayer graphene films were synthesized by a chemical vapor deposition method in a quartz tube using thermally-annealed copper foil (25-μm thick, 99.999% purity) as substrate [36, 37]. The graphene film on copper foil was examined by scanning electron microscopy (SEM; Nova nanoSEM 230) to ensure the highly crystalline and continuous features. Then, graphene films were transferred to quartz substrates using normal wet-transfer technology based on poly(methyl methacrylate) (PMMA) after etching away the copper foil with an aqueous solution of ammonium persulfate (0.01 g/L). The as-synthesized graphene films were characterized by optical microscopy, Raman and absorption spectroscopy. More detailed results and analyses can be found elsewhere [23]. The graphene film thickness (5~7 layers) were determined by a combination of spectroscopic techniques, namely, (i) reflection contrast spectroscopy (Nikon Eclipse Ti with a 50 × objective lens, tungsten halogen lamp), (ii) micro-Raman spectroscopy (WITec Alpha300R with an excitation wavelength of 532 nm and a 50 × objective lens), and (iii) NIR one-photon absorption spectroscopy (a Shimadzu UV-3600 UV−vis−NIR spectrophotometer). In the wavelength range of 1150 – 2400 nm, the absorbance of the film was in the range from 11% to 15%, in agreement with the monolayer absorbance (2.3%) multiplied by 5-7.

3. Nonlinear optical measurements

The nonlinear optical properties of our graphene sample were investigated using a Z-scan setup with a regeneratively amplified Ti:Sapphire source delivering ~100 fs pulses, pumping an optical parametric amplifier at a repetition rate of 1 kHz. The measurements are carried out in a broad range, ~1250 nm, at 4 different wavelengths: 1150, 1550, 1900 and 2400 nm, typical of Yb, Er, Tm and Cr:ZnSe lasers respectively. The beam was focused using a 200 mm focal length calcium fluoride lens after passing through a spatial filter in order to ensure its Gaussian shape. The sample was then translated through the focus along the beam path whilst recording the far-field transmittance through both open and closed aperture detectors. The waist of the beam was measured at each of the operating wavelengths using the knife-edge technique. It was found to be 25 μm at 1150 nm, 26 μm at 1550 nm, 28 μm at 2000 nm and 31 μm at 2400 nm.

For any given wavelength Z-scan measurements are undertaken at a range of pulse energies from 2 to 300 nJ which corresponded to irradiances from ~1 GWcm^{-2} to ~100 GWcm^{-2}. No laser induced damage was observed up to 100 GWcm^{-2}. Open-aperture measurements showed that the transmittance had a power dependence characteristic of saturable absorption in the relatively low-irradiance regime. As the input irradiance was increased, a rise in transmittance occurred due to saturable absorption, which was followed by a decrease in transmittance due to 2PA.

The competing SA and 2PA processes can be seen in Fig. 1 in which five consecutive Z-scans with increasing pulse energies at 1550 nm are presented. At the low pulse energy of 50 nJ, as the sample was translated through the focus of the beam, only a rise in transmittance was observed due to SA. However, as the pulse energy was increased further, a small valley started to form on top of the transmittance peak indicating the onset of 2PA.

#261726 Received 23 Mar 2016; revised 29 May 2016; accepted 30 May 2016; published 6 Jun 2016

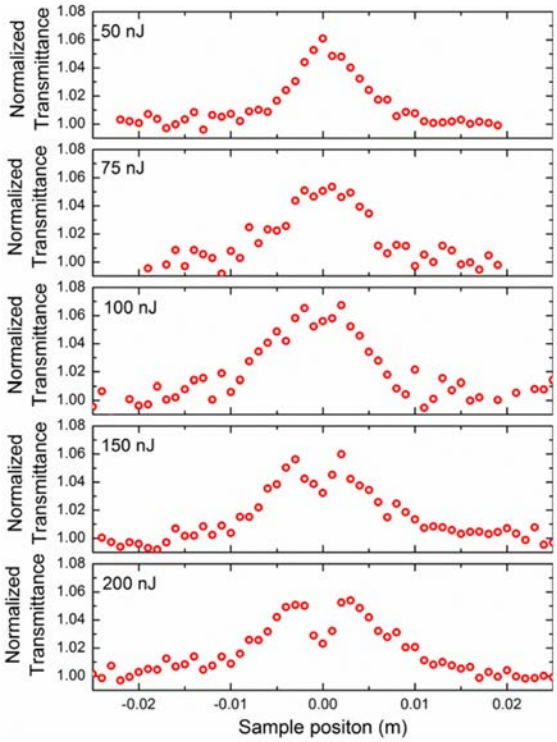

Fig. 1. Open aperture Z-scan traces at 5 consecutive pulse energies at 1550 nm showing the competitive saturable absorption and two-photon absorption processes.

At longer wavelengths the decrease in transmittance due to 2PA is more prominent; this suggests that there is a more significant contribution from 2PA due to the lower photon energy. At the highest irradiances investigated in this work, ~100 GWcm^{-2}, the transmittance decreased to about 0.99 for the case of 2400 nm while for the case of 1150 nm the decrease only reached 1.05. This behaviour can be seen in Fig. 2, where the irradiance versus normalized transmittance (at z = 0) is plotted for all 4 wavelengths.

The analytical expression used to fit the open aperture Z-scan measurements presented in Fig. 2 is obtained by numerically solving the propagation equation of a beam through a thin medium which presents both SA and 2PA following the method reported by Wang *et al.* [38]. The total nonlinear absorption coefficient $\alpha(I)$ at a given incident irradiance I is given by [21, 39–41]:

$$a(I) = \frac{a_0}{1+\frac{I}{I_{sat}}} + \beta I. \qquad (1)$$

In the above equation, α_0 is the linear absorption coefficient, I_{sat} is the saturation irradiance and β is the 2PA coefficient. Inspecting Eq. (1) one can deduce that the first and second terms describe SA and 2PA processes respectively.

#261726 Received 23 Mar 2016; revised 29 May 2016; accepted 30 May 2016; published 6 Jun 2016

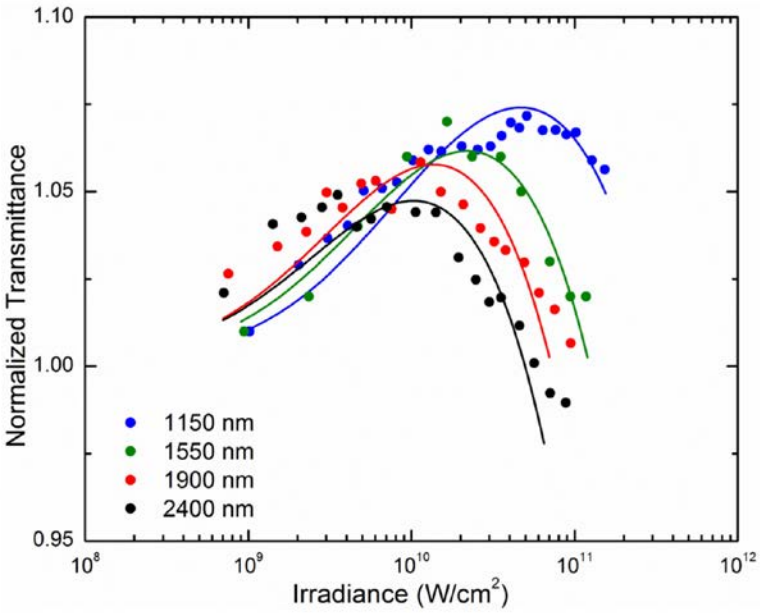

Fig. 2. Change in transmittance (at z = 0) with input irradiance at 1150, 1550, 1900 and 2400nm (dots) with the corresponding theoretical fits (solid lines).

The 2PA coefficient β and the saturation irradiance I_{sat} are extracted from the transmission numerical fits of Fig. 2. In the numerical simulation for the best fit, the α_0 parameter used is extracted from the linear transmission spectra of the sample at each of the operating wavelengths. The results are shown in Table 1. By inspecting this Table, a decrease in the saturation irradiance with longer wavelengths is observed. This is in very good qualitative agreement with the theoretical analysis performed in this paper. Furthermore, Yang *et al.* [21] observed the same wavelength dependence in bilayer graphene. Their reported values for the saturation irradiance are I_{sat} = 6 and 1.5 GWcm^{-2} at wavelengths of 780 and 1100 nm respectively, in very good agreement with our reported values in this work at longer wavelengths.

The 2PA coefficient β shows a small dependence on the wavelength, increasing with longer wavelengths. Yang *et al.* [21] reported giant 2PA in bilayer graphene with the same wavelength dependence as reported here. In addition, they derived a theoretical model showing the increase of β with longer wavelengths. Chen *et al.* [23] found the 2PA coefficient to be 16 cm/MW at 1100 nm in CVD-made 5-layer film of graphene, in good agreement with our reported values. The observed increase of β with wavelength, is also consistent with the theoretical prediction [21, 23] that the 2PA coefficient is proportional to $(h\nu)^{-4}$, where $h\nu$ is the photon energy. References [21, 23] treat graphene at visible and near-IR wavelengths, up to 1100 nm, in this work we have investigated the 2PA in graphene from 1150 nm up to 2400 nm. The simultaneous investigation of both SA and 2PA at longer wavelengths, and over a broad range, revealed the trend of the associated coefficients and the threshold at which SA turns to 2PA at this important wavelength region. This information will give insight in the optimum design of saturable absorbers for laser mode-locking in the wavelength region of ~1-2.5 μm.

#261726 Received 23 Mar 2016; revised 29 May 2016; accepted 30 May 2016; published 6 Jun 2016

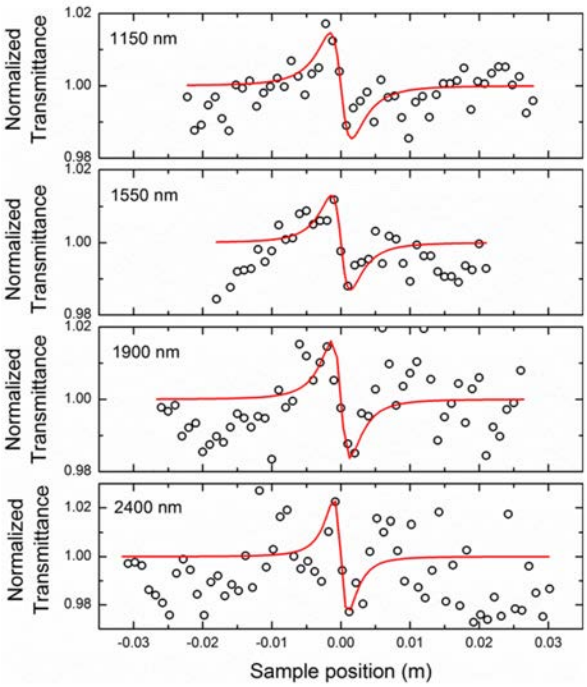

Fig. 3. Closed aperture Z-scan traces at 1150, 1550, 1900 and 2400 nm at an irradiance of 22 $GWcm^{-2}$ with the corresponding theoretical fits.

In addition, closed-aperture Z-scans were performed with a typical 50% aperture transmission. By introducing an iris in the beam path at the closed-aperture Z-scan regime, only an on-axis portion of the beam was collected. In this way the effect of the nonlinear phase shift can be measured; however, the effect of the absorptive nonlinearities is present in the closed-aperture trace too. In order to isolate the former from the latter, the closed aperture trace was divided by the open-aperture trace as explained by Sheik-Bahae *et al.* [24]. This yelded a typical closed-aperture Z-scan trace, one that would be obtained in the absence of any absorptive nonlinearities. The closed-aperture Z-scan traces at an irradiance of ~22 $GWcm^{-2}$ are shown in Fig. 3 for all four wavelengths. The traces were obtained after implementing the above described method of dividing the closed- by the open-aperture Z-scan traces, with no averaging or normalization performed after that. This explains why the data of Fig. 3 are noisier than the data of Fig. 1. As can be seen from Fig. 3, the observed nonlinear refraction has a negative sign. The theoretical fits in Fig. 3 use the simplified closed-aperture fitting formula from Sheik-Bahae *et al.* [24].

The values of the irradiance-dependent nonlinear refraction obtained from the fit for each wavelength are presented in Table 1. As can be seen graphene presents giant irradiance-dependent nonlinear refraction in the order of $\sim 10^{-9}$ cm^2W^{-1}. The order of magnitude for the n_2 coefficient reported in [25] was $\sim 10^{-7}$ cm^2W^{-1}; they obtained the n_2 value for irradiances lower than 0.1 $GWcm^{-2}$ before the nonlinear phase started saturating. In this work we operated in the nonlinear phase over-saturation regime, therefore measuring an irradiance-dependent nonlinear refraction $\tilde{n}(I)$. More specifically the Z-scans performed here were at irradiances of 22 $GWcm^{-2}$ about two orders of magnitude higher than the irradiances used in [25]. We obtained the irradiance-dependent nonlinear refraction coefficients for all of the operating wavelengths. The broad range at which the work was undertaken revealed for the first time the trend of the nonlinear refraction in graphene versus wavelength at such a wide range spanning ~1250 nm.

#261726 Received 23 Mar 2016; revised 29 May 2016; accepted 30 May 2016; published 6 Jun 2016

Table 1. Nonlinear Coefficients

Wavelength	α_o (m^{-1})	β (cm/GW)	I_{sat} (GW/cm^2)	$\tilde{n}(I)$ (cm^2/GW) at 22 $GWcm^{-2}$
1150nm	5.87×10^7	0.38×10^4	4.5	–0.55
1550nm	5.64×10^7	0.9×10^4	3	–0.8
1900nm	5.59×10^7	1.5×10^4	2.1	–1.4
2400nm	5.045×10^7	1.9×10^4	1.9	–2.5

4. Theoretical analysis

In this section we present theoretical results that lend support to the above experimental findings. We concentrate in particular on the conductivity, which can give important indications on the validity of the measurements of the nonlinear refraction effect for the multilayer graphene. The conductivity is usually written for monochromatic waves; however, one can perform useful estimates with it, even in the case of short pulses.

The analytical expression of the complex linear conductivity $\sigma(\omega)$ of a graphene monolayer is known from Falkovsky's work [42]:

$$\sigma(\omega)=\frac{ie^2(2k_BT)}{\pi\hbar^2(\omega+i\gamma_1)}\left[\frac{E_F}{2k_BT}+\log\left(2e^{-\frac{E_F}{k_BT}}+1\right)\right]+$$
$$\frac{e^2}{4\hbar}\left\{\frac{1}{2}+\frac{1}{\pi}\arctan\left[\frac{\hbar(\omega+i\gamma_2)-2E_F}{2k_BT}\right]\right\}-\frac{i}{2\pi}\log\left\{\frac{\left[\hbar(\omega+i\gamma_2)-2E_F\right]^2}{\left[\hbar(\omega+i\gamma_2)-2E_F\right]^2+(2k_BT)^2}\right\}. \quad (2)$$

where T is the temperature, k_B is the Boltzmann constant, E_F is the Fermi energy (chemical potential), γ_1 and γ_2 are the inverse relaxation times [43]. At zero temperature and in the case of photoexcited undoped graphene where $E_F=0$, the conductivity

$$\sigma(\omega)=\sigma_0=\frac{e^2}{4\hbar}. \quad (3)$$

is purely real, and equal to the value for the universal conductivity of monolayer graphene. We now generalize Eq. (2) to the nonlinear case and for a multilayer graphene made of *N* layers. We basically model our multilayer as a single layer with an effective thickness such that the linear absorption coefficient α_0, which is due to the *N* graphene layers plus the substrate, matches the experimentally observed one over the range of wavelengths relevant to our experiments.

Here we take the values $1/\gamma_1 \approx 400\,\text{fs}$ and $1/\gamma_2 \approx 20\,\text{fs}$, in order to fit the measured values of the linear absorption coefficient α_0 in Table 1. These values are effective and strongly depend on the number of layers and the type of substrate employed. In the case of photoexcited undoped graphene the Fermi energy vanishes, $E_F=0$.

The relation between the complex linear susceptibility and the conductivity in the multilayer graphene sample is taken to be simply as

$$\chi(\omega)=\frac{iN\sigma(\omega)}{\varepsilon_0\omega d_{eff}}=\chi'+i\chi''. \quad (4)$$

#261726 Received 23 Mar 2016; revised 29 May 2016; accepted 30 May 2016; published 6 Jun 2016

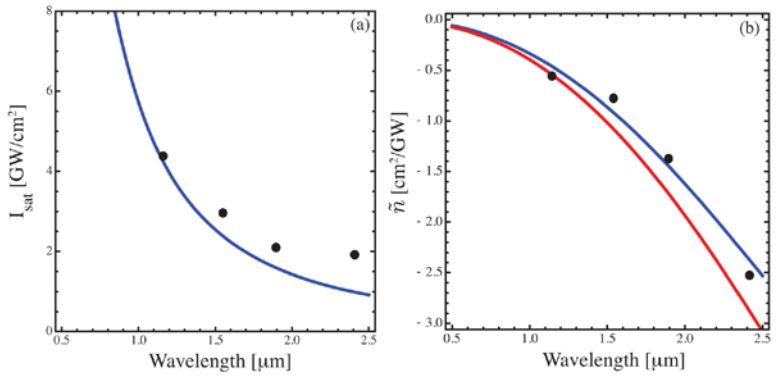

Fig. 4. (a) Total saturation irradiance I_{sat} versus wavelength, in conditions of room temperature along with the experimental values from Table 1 (black dots); (b) Real (blue line) and imaginary (red line) parts of the nonlinear refractive index versus wavelength at 22 GWcm^{-2} along with the experimental values from Table 1 (black dots).

where d_{eff} is the effective thickness of the multilayer, which represents the combined thickness of each graphene layer in the multilayer and the contribution from the substrate. In our estimates we assume $N = 7$ layers, and we find that $d_{eff} \approx 8d$, where $d = 0.33$ nm is the monolayer graphene thickness, fits well with the absorption data of our experiments.

The theoretical value for the saturation irradiance is found by using the semiconductor Bloch equations [44] adapted to the graphene dispersion, and generalized for N layers. In particular, the rate equation (which is identical for the case of semiconductors and graphene, since it does not depend on the electronic dispersion [44]) gives the following formula:

$$I_{sat} = Nc\varepsilon_0\gamma_1\gamma_2\left(\frac{\hbar\omega_0}{ev_F}\right)^2. \tag{5}$$

where v_F is the Fermi velocity and ω_0 is the central pulse frequency in the CW approximation. The wavelength dependence of I_{sat} is plotted in Fig. 4(a) and qualitatively agrees well with the values in Table 1, also presented in 4 (a). The quantitative discrepancies observed with the experimental values are attributed to the fact that in the theoretical prediction the 2PA is neglected and the CW approximation for the conductivity is used.

Using the full nonlinear susceptibility (that can be derived by solving the rate equation of the semiconductor Bloch equations [44]) given by:

$$\chi(\omega) = \frac{iN\sigma(\omega)}{\varepsilon_0\omega d_{eff}}\frac{1}{\left(1+\frac{I}{I_{sat}}\right)}. \tag{6}$$

in which the denominator is common to all rate equations based on two-level systems, we obtain

$$n(I) + ik(I) = \sqrt{1+\chi(\omega)}. \tag{7}$$

where $n(I)$ is the irradiance-dependent refractive index and $k(I)$ is the irradiance-dependent extinction coefficient responsible for absorption. One can define the nonlinear refraction coefficient $\tilde{n}(I) = \partial n / \partial I$. This coefficient has the same physical dimension of the conventionally used nonlinear refractive index n_2, but a different meaning: n_2 is a coefficient

#261726 Received 23 Mar 2016; revised 29 May 2016; accepted 30 May 2016; published 6 Jun 2016

in the Taylor expansion of the nonlinear refractive index calculated at I = 0, which is independent of the irradiance in accordance with our earlier statement. However, $\tilde{n}(I)$ is an irradiance-dependent function that gives the slope of the nonlinear refraction versus irradiance diagram, and is not connected to any perturbative expansion. It is $\tilde{n}(I)$ that the Z-scan provides in our measurements. Note that here a truncated Taylor expansion is not applicable since in our experiments we operate in the over-saturation regime $(I \gg I_{sat})$, where the nonlinearity is non-perturbative. As a consequence, any measurement of the nonlinear refraction coefficient in graphene will strongly depend on the particular irradiance used. Thus, under conditions of oversaturation, the nonlinear refractive index coefficients do not decrease, the conventional (truncated) Taylor series diverges, and the interpretation of n_2 must be modified according to the above formulae and discussion. The calculated irradiance-dependent nonlinear refraction coefficient $\tilde{n}(I)$, both real and imaginary part, is plotted in Fig. 4(b) against wavelength at 22 GWcm^{-2} along with the experimental values from Table 1. Note that $\chi_{gr}^{(3)}$ and $\tilde{n}(I)$ can in general have the same or opposite signs, depending on the frequency, since $\chi_{gr}^{(3)}$ is complex, the relationship between them is not just a simple proportionality factor.

Despite the fact that the 2PA is neglected and the CW conductivity of Eq. (4) is used, it is remarkable to observe that the values extracted from the plot of Fig. 4(b) are in excellent qualitative agreement with Table 1. Most importantly, it can be seen that the nonlinear refraction coefficient is negative for a broad region of frequencies, as also pointed out by Ooi [28], albeit in the case of doped graphene and thus for non-vanishing Fermi energy. The imaginary part of $\tilde{n}(I)$ is also negative, which is natural since nonlinearity reduces the linear losses due to the saturation process.

5. Conclusions

In this paper we studied the nonlinear optical properties of multilayer graphene by Z-scan. The saturable absorption, two-photon absorption, and nonlinear refraction properties were studied in the femtosecond temporal regime for a broad range of wavelengths, namely 1150, 1550, 1900 and 2400 nm. The saturation irradiances, I_{sat}, and the two-photon absorption coefficients, β, were measured in the operating wavelength range. Furthermore, a negative irradiance-dependent nonlinear refraction was observed. This irradiance-dependent nonlinear refraction was symbolized with $\tilde{n}(I)$ and discriminated from the conventional nonlinear refraction coefficient n_2, which is irradiance-independent. A theoretical analysis arising from the conductivity of the graphene monolayer along with a thermal analysis based on the laser parameters used, verify that the negative value of the nonlinear refraction arises from the graphene multilayer. This is the first time that the nonlinear refractive effect in graphene is studied over a broad wavelength range. The values obtained for $\tilde{n}(I)$ show that graphene presents giant nonlinear refraction in the order of ~10^{-9} cm^{2}W^{-1}, approximately 8 orders of magnitude larger than bulk dielectrics. The work performed here provides a fast and accurate way for characterizing graphene-based materials for the development of graphene-based nonlinear photonic devices in the infrared up to 2.5 μm.

Acknowledgments

Heriot Watt University authors would like to acknowledge financial support from the UK Engineering and Physical Sciences Research Council (EPSRC), Grant number EP/G030227/1. The work of G Demetriou was supported by a James Watt scholarship from Heriot-Watt University. The National University of Singapore author would acknowledge financial support from the Ministry of Education, Singapore Grant Number R-144-000-327-112.

#261726 Received 23 Mar 2016; revised 29 May 2016; accepted 30 May 2016; published 6 Jun 2016